Research Article

MOLECULAR PAIN

Molecular Pain
Volume 12: 1–13

DOI: 10.1177/1744806916674472
mpx.sagepub.com
SAGE

A painful neuropathy-associated Nav1.7 mutant leads to time-dependent degeneration of small-diameter axons associated with intracellular Ca^{2+} dysregulation and decrease in ATP levels

Harshvardhan Rolyan, PhD[1,2], Shujun Liu, MD[1,2], Janneke GJ Hoeijmakers, MD, PhD[3], Catharina G Faber, MD, PhD[3], Ingemar SJ Merkies, MD, PhD[3,4], Giuseppe Lauria, MD, PhD[5], Joel A Black, PhD[1,2] and Stephen G Waxman, MD, PhD[1,2]

Abstract

Small fiber neuropathy is a painful sensory nervous system disorder characterized by damage to unmyelinated C- and thinly myelinated Aδ- nerve fibers, clinically manifested by burning pain in the distal extremities and dysautonomia. The clinical onset in adulthood suggests a time-dependent process. The mechanisms that underlie nerve fiber injury in small fiber neuropathy are incompletely understood, although roles for energetic stress have been suggested. In the present study, we report time-dependent degeneration of neurites from dorsal root ganglia neurons in culture expressing small fiber neuropathy-associated G856D mutant Nav1.7 channels and demonstrate a time-dependent increase in intracellular calcium levels $[Ca^{2+}]_i$ and reactive oxygen species, together with a decrease in ATP levels. Together with a previous clinical report of burning pain in the feet and hands associated with reduced levels of Na^+/K^+-ATPase in humans with high altitude sickness, the present results link energetic stress and reactive oxygen species production with the development of a painful neuropathy that preferentially affects small-diameter axons.

Keywords

ATP, axon degeneration, mitochondria, peripheral neuropathy, reactive oxygen species, sodium-calcium exchanger, voltage-gated sodium channel

Date received: 12 July 2016; revised: 10 August 2016; accepted: 16 August 2016

Introduction

Small fiber neuropathy (SFN) is characterized by injury to unmyelinated C-fibers and thinly myelinated Aδ-fibers and a loss of small-diameter intra-epidermal nerve fibers (IENF), producing sensory and autonomic abnormalities.[1–4] SFN can occur as an accompaniment of multiple conditions, including diabetes mellitus and impaired glucose tolerance, systemic immune-mediated diseases, cancer chemotherapy, and infectious processes, but in 24%–93% of cases of SFN, there is no apparent non-genetic cause.[5,6] Faber et al.[7] reported gain-of-function mutations in voltage-gated sodium channel Nav1.7 (SCN9A) in nearly 30% of patients with idiopathic biopsy-confirmed, painful SFN. Subsequently,

[1]Department of Neurology, Yale University School of Medicine, New Haven, CT, USA
[2]Neuroscience and Regeneration Research Center, VA Connecticut Healthcare System, West Haven, CT, USA
[3]Department of Neurology, Maastricht University Medical Center, Maastricht, The Netherlands
[4]Department of Neurology, St. Elisabeth Hospital, Willemstad, Curaçao
[5]Neuroalgology Unit, IRCCS, Carlo Besta Neurological Institute, Milan, Italy

Corresponding author:
Stephen G Waxman, Department of Neurology, Yale University School of Medicine, Veterans Affairs Medical Center, Neuroscience Research, Bldg. 34, West Haven, CT 06516, USA.
Email: Stephen.waxman@yale.edu

additional SFN-associated gain-of-function mutations have been identified in SCN9A,[8,9] in SCN10A (the gene encoding Nav1.8),[10–12] and SCN11A (the gene encoding Nav1.9).[13,14]

Nav1.7 mutation G856D (c.2567G > A) was identified in a multi-generational family whose affected members experience SFN-associated symptoms, including severe pain in the distal extremities.[9] Functional analyses demonstrated that the G856D mutation significantly alters the biophysical properties of the Nav1.7 channel, producing hyperpolarization of activation, depolarization of steady-state fast inactivation, slow deactivation, and markedly enhanced persistent current.[9] The altered biophysical properties of the mutant Nav1.7 channel depolarize dorsal root ganglia (DRG) neurons and make them hyperexcitable, as manifested by reduced current threshold, increased frequency of firing in response to subthreshold stimulation, and increased spontaneous firing.

In contrast to neurites of DRG neurons expressing wild-type (WT) Nav1.7 channels, neurites of DRG neurons expressing mutant G856D channels display substantial degeneration when pre-conditioned *in vitro* by depolarization and metabolic challenge.[15] Previous work in small-diameter white matter axons subjected to anoxia has shown that increased inward Na^+ flux through incompletely inactivating sodium channels can lead to reversal of the sodium-calcium exchanger (NCX) and import of damaging levels of Ca^{2+}.[16] Estacion et al.[15] recently showed that the increased levels of $[Ca^{2+}]_i$ in G856D-expressing neurites results from enhanced Na^+ influx through mutant Nav1.7 channels and reverse operation of the NCX. Increased levels of intracellular $[Ca^{2+}]$ have been linked to initiation of degradative pathways and axonal degeneration through activation of calpains, phospholipases, and nitric acid synthases (see literature[17]).

In humans, SFN generally progresses in an age-dependent manner[18] with symptoms usually appearing at least a decade after birth, despite the presence throughout life of gain-of-function mutations of sodium channels.[7,10,13] These observations suggest that enhanced Na^+ influx through mutant Nav1.7 channels may confer an accumulating energetic burden on axons, particularly on small-diameter unmyelinated axons (i.e. IENF), which are preferentially sensitive to small changes in ion channel activity due to their high surface-to-volume ratio, high input resistance, and short diffusional and electrotonic length constant.[19,20] In this study, we assayed time-dependent changes in intracellular $[Ca^{2+}]_i$ levels, degeneration and energetic stress in the neurites of DRG neurons expressing mutant G856D Nav1.7 channels. Our results provide mechanistic evidence for a time-dependent increase in intracellular $[Ca^{2+}]_i$ and energetic compromise in the neurites of DRG neurons expressing G856D mutant channels.

Materials and methods

Expression constructs

The expression constructs for WT and G856D mutant forms of human Nav1.7 pore-forming α- subunit (adult isoform containing exon 5) have been described previously.[9] The functional activity of the clones used in this study was confirmed by electrophysiology on transfected HEK cells.

Isolation and culture of primary DRG neurons

All animal protocols were approved by the Institutional Animal Care and Use Committee of the VA Connecticut Healthcare System, and all experiments were carried out in accordance with guidelines for the care and use of laboratory animals from National Institutes of Health. Isolation and culture of DRG neurons were performed as described previously,[15] with slight modifications. Briefly, 4–6-week-old male Sprague-Dawley rats (Charles River, USA) were anesthetized with CO_2 narcosis and decapitated; 14 DRG from each animal were surgically removed and placed in ice-cold complete saline solution (CSS; containing 137 mM NaCl, 5.3 mM KCl, 1 mM $MgCl_2$, 25 mM Sorbitol, 3 mM $CaCl_2$, and 10 mM HEPES; pH 7.2, osmolarity 315 mOsm/L). DRG were pooled from two animals and after careful removal of meninges were enzymatically digested with Collagenase A ((70474031, Roche) 1.5 mg/ml in CSS containing 0.6 mM ethylene diamine tetraacetic acid) for 15 min at 37°C with mild agitation, followed by Collagenase D ((70507821, Roche) 1.5 mg/ml in CSS, containing 30 U/ml Papain (LS003126, Worthington Biochemical) and 0.6 mM ethylene diamine tetraacetic acid) for 15 min at 37°C with mild agitation. Digested ganglia were gently triturated in two steps with wide-bore pipette tips (T-205-WB-C-R-S, Axygen) in 500 µl DRG media (DMEM/F12 (11320, Gibco) supplemented with 100 U/ml penicillin, 0.1 mg/ml streptomycin, and 10% fetal bovine serum (SH3008, HyClone) containing 1.5 mg/ml trypsin inhibitor (T9253, Sigma) and 1.5 mg/ml bovine serum albumin (BSA; A8806, Sigma). The triturated cell suspension was layered over 5 ml of 15% BSA (A9418, Sigma) in DRG media to form a gradient and centrifuged at 200 relative centrifugal force for 10 min to remove the non-neuronal cells.[21] The neuron-enriched cell pellet was re-suspended in 40 µl transfection reagent (Amaxa, Basic Neuron SCN Nucleofector kit, VSPI-1003, Lonza) to permit electroporation.

Transfection of DRG neurons

After enrichment, the dissociated DRG neurons were transfected by electroporation with the WT and G856D mutant Nav1.7 expression constructs along

with either enhanced green fluorescent protein (GFP) or mCherry (mCh) as a fluorescent reporter, using the nucleofector II system (program 6, Amaxa). After re-suspending the cells in transfection reagent, the cell suspension was split into two equal volumes of 20 µl and 2 µl of Nav1.7 construct DNA (stock 1 µg/µl), and 0.2 µl of marker DNA (stock 0.5 µg/µl) was mixed (Nav1.7 to marker ratio 20:1). After electroporation, cells were allowed to recover for 10 min at 37°C in 0.2 ml of pre-warmed Ca^{2+} free DMEM (21068, Gibco). The cell suspension was added with 1.2 ml of pre-warmed DRG media containing 1.5 mg/ml trypsin inhibitor and 1.5 mg/ml BSA; 100 µl of this cell suspension was plated on 14 mm laminin-coated (L2020, Sigma) and poly-d-lysine pre-coated glass bottom dishes (P35GC-1.5-14-C, MatTek Corp.) in a circular "donut" forming distribution (donut culture) and incubated at 37°C and 5% CO_2. One hour later, 1.0 ml of DRG media supplemented with 50 ng/ml NGF (N-240, Alomone Labs) and 50 ng/ml GDNF (450-10, Peprotech) was gently added, and cells were maintained at 37°C in a 5% CO_2 incubator. The following day, DRG media was replaced with neurobasal A medium (A1371001, Gibco) containing 100 U/ml penicillin, 0.1 mg/ml streptomycin, 2.5 mM l-glutamine, 1X B27 supplement (17504, Gibco), and 50 ng/ml of NGF and GDNF. To inhibit the growth of non-neuronal cells, anti-mitotic reagent 5-fluoro-2′-deoxyuridine (F0503, Sigma) and uridine (U30003, Sigma) were added in the culture media at a concentration of 10 µM each for one week and thereafter at a lower concentration of 1 µM. The culture media was changed every week, and throughout the experiment, cells were kept at 37°C and 5% CO_2 inside a humidified incubator. For determining the viability of transfected DRG neurons, Live-Dead assay kit (R37601, Molecular Probes) was used as per manufacture recommended guidelines.

Donut culture of DRG neurons

Figure 1 illustrates the seeding methods and distribution of DRG neurons on the laminin-coated and poly-d-lysine pre-coated glass culture surface. The standard dispersed seeding method for culturing DRG neurons usually leads to clustering, especially towards the center of the coated coverslip. The formation of neurites (both density and length) is affected by clustering behavior; while neurons in a cluster grow neurites extensively, the distantly isolated neurons do not (data not shown). The donut seeding method, which involves plating cells in donut-like distribution leaving a small void at the center, provides a uniform distribution of DRG neurons on the culture surface and improves neurite formation as well as quantification by the neurite tracer plugin in Image J.

Live cell imaging

Imaging was performed on live DRG neurons on multiple days in culture (days in vitro (DIV)), using Nikon Eclipse Ti microscopes fitted with environmentally controlled chambers (InVivo Scientific, St Louis, MO) to maintain cells at 37°C temperature and 5% CO_2 inside a humidified environment. Images were acquired using NIS-Elements software (Nikon). For all imaging purposes, phenol red-free Neurobasal A medium was used (12349015, Gibco).

Neurite analysis

For quantification of neurite lengths, large-field montage images covering the entire culture area of the glass bottom dish were acquired using a motorized stage and 20× objective of live DRG neuronal cultures. For image processing and neurite length measurements, NeuriteTracer plugin was used in Image J (version 1.48, National Institutes of Health, Bethesda, MD).[22] Images were converted to binary, and threshold levels were set based on GFP signal intensity to create two binary images, one including cell bodies as well as neurites (neuronal) and another only cell bodies (nuclear). For each montage image, total neurite length was calculated and divided by the total number of neurons, which were counted separately using the particle analyzer module in Image J. In each experiment, neurite lengths for cells expressing the mutant G856D channel were normalized and expressed as a percentage of the length for sister cultures containing WT-expressing DRG neurons, prepared concurrently from the same preparation of DRGs. For each time point, one large image from a single culture dish (5–8 dishes per culture) was analyzed from at least three different cultures. For quantification of degenerating neurites transfected with Nav1.7 WT and G856D constructs, neurite segments were considered degenerating if they displayed signs of fragmentation and/or repetitive blebbing and were counted visually as a percentage to the total GFP-expressing neurites in the image. Four to five images at 40× magnification were acquired and analyzed from random areas spanning the entire culture dish, and at least three to five dishes were analyzed from three different cultures.

Intracellular calcium imaging

Intracellular calcium levels $[Ca^{2+}]_i$ were measured using the cell permeable, acetoxymethyl ester (AM) derivative of the ratio-metric calcium indicator fura2 (F1221, Molecular Probes). DRG neurons cultured for 3, 15, and 30 DIV were loaded with 2 µM fura2-AM and 0.02% Pluronic detergent (540025, Calbiochem) in standard bath solution (SBS; containing 140 mM NaCl,

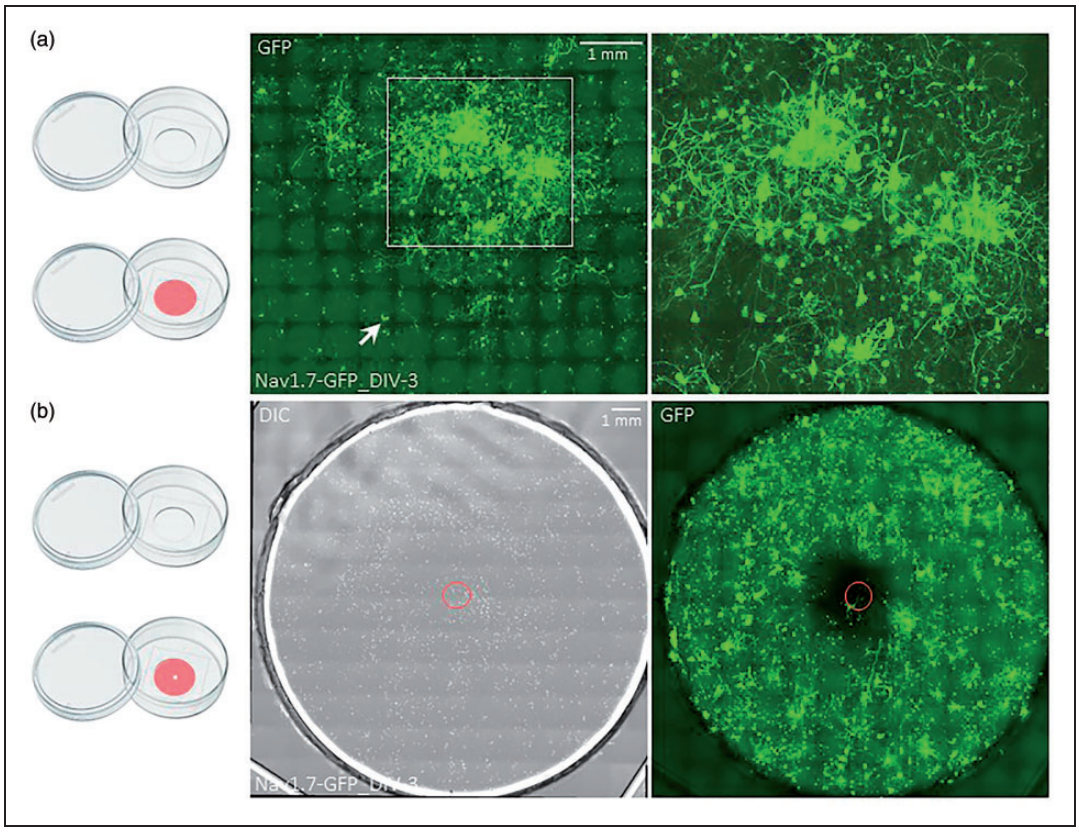

Figure 1. Culture of primary rat DRG neurons. Representative images describing the seeding methods and distribution of DRG neurons on the coated glass culture surface. (a) The standard method of seeding cells often leads to clustering of DRG neurons in culture. The middle image shows that formation of neurites (both density and length) is affected by the clustering behavior. Neurons in a cluster can grow extensive neurites (boxed area, enlarged on right), while isolated neurons generally do not (arrow). This distribution of neurons can result in experimental variability and an inability to process images for neurite quantification. (b) The donut seeding method plates DRG neurons in a "donut-like" pattern and leaves a small void at the center of the culture surface (indicated by the small circle). This manner of plating provides a uniform distribution of DRG neurons on the coated culture surface. Phase contrast (middle panel) and GFP fluorescent signal (right panel) images of transfected neurons and neurites of the same culture dish are shown. Note the differences in distribution of neurons and neurite formation displayed by the standard method and donut-like method of plating.
GFP: green fluorescent protein; DIV: days in vitro.

3 mM KCl, 1 mM $MgCl_2$, 1 mM $CaCl_2$, and 10 mM HEPES; pH 7.2, osmolarity 310 mOsm/L) and incubated for 45 min at 37°C inside a 5% CO_2 incubator. After gentle washing with SBS and another 30 min incubation, images were acquired from live cells. Transfected neurites were identified by expression of mCherry, which was co-transfected with Nav1.7 WT or G6856D constructs. Cultures were alternatively illuminated every 200 ms with 340 nm and 380 nm wavelength light from a fast switching xenon light source (Lambda DG-4, Sutter Instruments). Images were acquired using a Nikon Ti-E inverted microscope equipped with a QuantEM CCD camera (Princeton Instruments) and a UV permissive objective (Super Fluor, Nikon). Intracellular calcium levels $[Ca^{2+}]_i$ were measured as a ratio of fluorescence signal at 340 nm and 380 nm (F_{340}/F_{380}) excitation wavelengths after background subtraction by overlaying neuronal cell bodies and neurites with defined regions of interest (ROI) markers, using NIS-Elements software (Nikon). Thin and thick neurites were defined by their diameters (thin neurites $< 3\mu m$, thick neurites $> 5\mu m$) and identified by overlaying with a size marker.

Intracellular ATP analysis

Assessment of neurite ATP levels was performed by utilizing a cell permeable AM ester derivative of magnesium green (MgGreen) as an indicator dye (M3735, Molecular Probes). ATP binds to magnesium with higher affinity than ADP, and cytosolic magnesium concentration $[Mg^{2+}]_i$ rises upon ATP hydrolysis. Based on this principle, intracellular ATP levels have been previously measured in inverse correlation with $[Mg^{2+}]_i$ levels.[23] Briefly, cells were loaded with 1 μM MgGreen-AM and 0.02%

Pluronic detergent in phenol red-free growth media and incubated for 1 hr at 37°C inside a 5% CO_2 incubator, followed by gentle washing and another 30 min incubation inside the incubator. Intracellular ATP levels were assessed in inverse correlation to MgGreen fluorescence intensity after background correction by overlaying neurites with defined ROI markers using NIS-Elements software.

Analysis for reactive oxygen species

Reactive oxygen species (ROS) were measured with the general oxidative stress indicator dye CM-H2DCFDA (C6827, Molecular Probes), which is suitable for intracellular measurements of ROS. CM-H2DCFDA is oxidized by ROS, and the oxidized product produces intense green fluorescence. Briefly, DRG neurons cultured for 3, 15, and 30 DIV were loaded with 5 μM CM-H2DCFDA and 0.02% Pluronic detergent in phenol red-free culture media and incubated for 30 min at 37°C inside a 5% CO_2 incubator, followed by gentle washing and imaging. Intracellular ROS levels were assessed in direct correlation to the fluorescence intensity after background correction and measured by overlaying neurites with defined ROI markers using NIS-Elements software.

Statistical analysis

All results are expressed as mean values ± SEM from a set of replicate experiments at each time point. Comparison between WT and G856D was analyzed by unpaired Student's *t* test with unequal variance, and *P* values less than 0.05 were considered statistically significant.

Results

Time-dependent decrease in lengths of neurites expressing the SFN-associated G856D Nav1.7 mutant channels

SFN is generally associated with a loss of small caliber IENF.[1] To determine the effect of Nav1.7 mutant channels on the neurites of DRG neurons, we expressed WT and G856D mutant Nav1.7 channels in DRG neurons *in vitro* and compared the neurite lengths after three days in culture. At three DIV, the average neurite length of DRG neurons expressing G856D mutant Nav1.7 channels was 97.46 ± 6.22% relative to 100 ± 3.92% for the WT Nav1.7 channels (P = ns, Figure 2(a) and (c)).

SFN is characterized by age-dependent disease progression. Therefore, we also compared neurite lengths from DRG neurons expressing the WT and G856D mutant Nav1.7 channels at a later time point of 30 DIV culture. At 30 DIV, the average neurite length from DRG neurons expressing the G856D mutant Nav1.7 was 70.54 ± 3.33% relative to 100 ± 2.31% for the WT Nav1.7 ($P < 0.001$, Figure 2(a) and (c)), indicating a time-dependent decrease in neurite lengths expressing G856D mutant channels.

Time-dependent degeneration of small-diameter neurites expressing G856D mutant Nav1.7 channels

To examine molecular pathways that contribute to the time-dependent decrease in neurite lengths of G856D/Nav1.7-expressing DRG neurons, we quantified the frequency of degenerating neurites of DRG neuron cultures, expressing the WT and G856D mutant Nav1.7 channels. The average frequency of degenerating neurites of DRG neurons at three days in culture was 1.52 ± 0.33% for WT Nav1.7 and 1.60 ± 0.29% for the G856D mutant Nav1.7 channels (P = ns, Figure 2(a) and (d)). At 30 days in culture, the average frequency of degenerating neurites from DRG neurons expressing WT Nav1.7 was 11.57 ± 0.59% in comparison to 30.92 ± 1.78% for DRG neurons expressing G856D mutant Nav1.7 channels ($P < 0.001$, Figure 2(a) and (d)). Moreover, thin (<3 μm diameter) neurites exhibited a nearly four-fold greater percentage of degenerating neurites than thick (>5 μm diameter) neurites (Figure 2(f); thin: 78.12% vs. thick: 21.88%). The significant increase in the frequency of degenerating neurites from DRG neurons expressing the G856D mutant Nav1.7 channels and maintained for 30 DIV suggests that the expression of the G856D mutant channel can lead to degeneration of neurites *in vitro* in a time-dependent manner.

These results demonstrate time-dependent development of axonal injury in DRG neurons expressing G856D channels. To rule out the possibility that this was due to degeneration of DRG neurons, we assessed DRG neurons using a live/dead cell assay. The significant decrease in neurite lengths and increase in frequency of degenerating neurites were not associated with a decrease in viability of neurons expressing the G856D mutant Nav1.7 channels (Figure 2(e)).

Elevated intracellular calcium levels in small-diameter neurites expressing G856D Nav1.7mutant channels

To determine whether neuronal cell bodies and neurites exhibit differential levels of $[Ca^{2+}]_i$, we compared $[Ca^{2+}]_i$ levels from healthy appearing neurites that did not show signs of degeneration and also cell bodies of the DRG neurons expressing WT and G856D mutant Nav1.7 channels at different times in culture. By using the ratiometric calcium indicator fura2, we observed significantly higher levels of $[Ca^{2+}]_i$ in small-diameter neurites

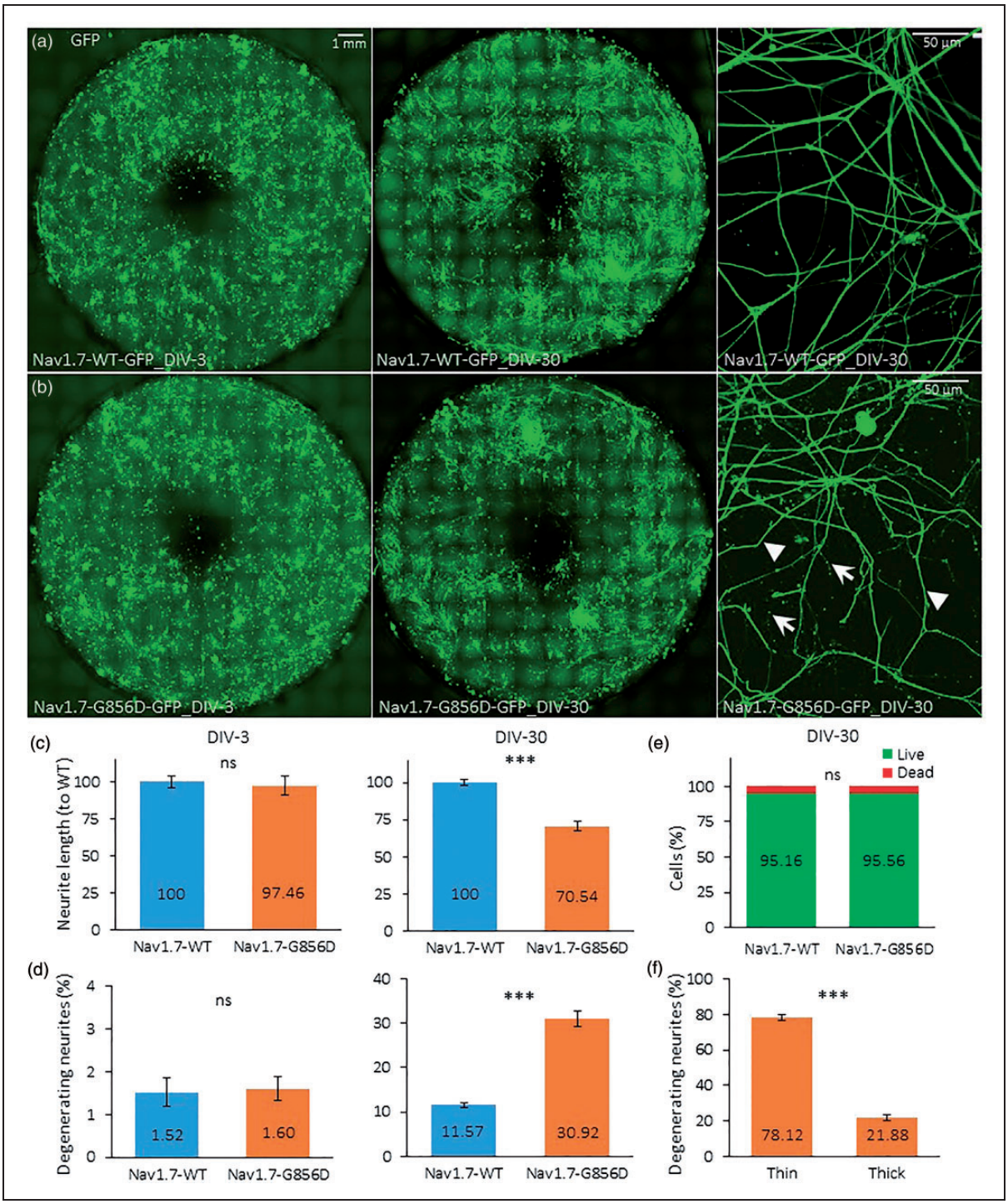

Figure 2. Neurite degeneration in DRG neurons expressing WT and mutant G856D Nav1.7 channels. Representative images of DRG neurons expressing wild type (WT) (a) and G856D mutant (b) Nav1.7 channels and GFP at three days (left panel) and 30 days (middle panel) *in vitro*. Images on right panels show WT and G856D expressing neurites at 30 days in culture at increased magnification. Arrows denote signs of degeneration (blebbing and fragmentation) in small-diameter (<3 µm) neurites expressing G856D; in contrast, larger diameter (>5 µm) neurites expressing G856D are relatively unaffected (arrowheads). Small and larger diameter neurites expressing WT Nav1.7 channels exhibit limited degeneration. (c) Histograms showing neurite length (average length relative to WT control) of DRG neurons expressing the WT and G856D mutant Nav1.7 channels at three days and 30 days *in vitro*. Note the reduction in neurite lengths of DRG neurons expressing the G856D mutant at 30 days in culture compared to WT channels. (d) Histograms showing frequency of degenerating neurites expressing WT and G856D Nav1.7 channels after three days and 30 days *in vitro*. The frequency of degenerating neurites was low and not significantly different between WT and G856D expressing neurons at three days in culture. In contrast, at 30 days

(<3.0 μm; thin) expressing G856D mutant Nav1.7 channels at 30 DIV as compared to thin diameter neurites expressing WT Nav1.7 channels ($P = 0.0082$, Figure 3(c)). In contrast, at 30 DIV, thick neurites (>5.0 μm in diameter) and neuronal cell bodies expressing the WT and G856D Nav1.7 channels did not exhibit significant differences in $[Ca^{2+}]_i$ levels (Figure 3(c)). Specifically, at three DIV, significant differences in $[Ca^{2+}]_i$ levels in the neurites of either < 3.0 μm or > 5.0 μm diameter were not detected (Figure 3(b)). At three days, the average fluorescence intensity ratio of fura2 (F_{340}/F_{380}) of neurites < 3.0 μm diameter (thin) was 0.8401 ± 0.0256 for WT Nav1.7 and 0.8732 ± 0.0439 for G856D Nav1.7 ($P = 0.5333$, Figure 3(b)), and for

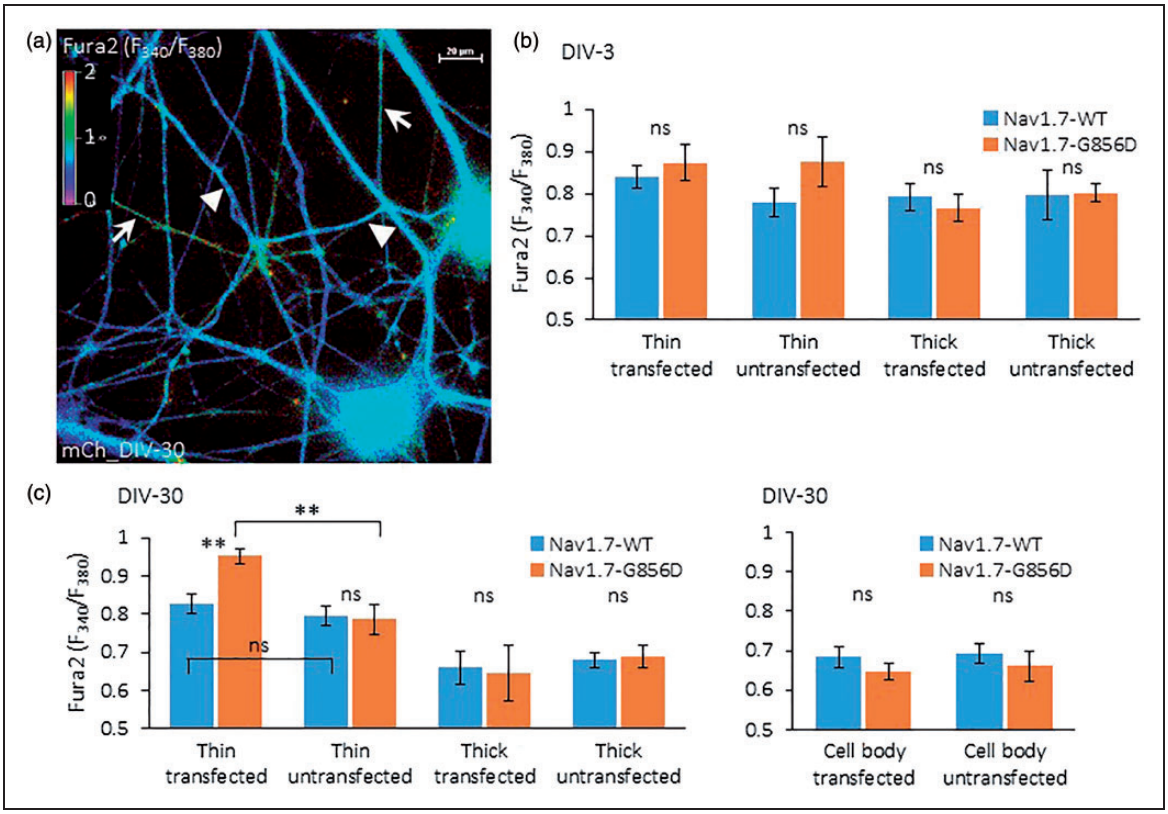

Figure 3. Intracellular calcium levels in neurites expressing WT and G856D Nav1.7 channels. (a) A representative image showing the ratio of fura2 emission signals at 340 nm and 380 nm excitation wavelengths (F_{340}/F_{380}) of DRG neurons at 30 days in vitro. The color bar denotes the F_{340}/F_{380} values (0–2), with higher levels of $[Ca^{2+}]_i$ indicated at the far red end of the spectrum. Arrowheads point to larger diameter neurites that are color-coded towards the blue end of the spectrum (lower $[Ca^{2+}]_i$ levels), and arrows point to the smaller diameter neurites that are color-coded towards the red end of the spectrum (higher $[Ca^{2+}]_i$ levels). (b) and (c) Histograms showing the average F_{340}/F_{380} values of neurites transfected with WT and G856D mutant Nav1.7 channels or neurites in the cultures that are untransfected after three days (b) and 30 days (c) *in vitro*. Thin and thick neurites are defined as < 3 μm or > 5 μm in diameter, respectively. Significant differences were not observed between any groups of neurites at three days in culture. In contrast, at 30 days *in vitro*, $[Ca^{2+}]_i$ levels (assayed by F_{340}/F_{380} values) were significantly higher in thin neurites expressing the G856D mutant Nav1.7 in comparison to the WT Nav1.7 expressing neurites ($P = 0.0082$). The F_{340}/F_{380} values were not significantly different between thick neurites expressing WT and G856D channels or between neuronal cell bodies expressing WT and G856D channels.

Figure 2. Continued
in culture, the frequency of degenerating neurites was approximately three-fold greater in neurons expressing G856D in comparison to WT channels. (e) Histogram showing Live/Dead assay viability of WT and G856D transfected DRG neurons at 30 days in culture. Approximately 95% of both WT and G856D expressing neurons were viable at 30 days in vitro. (f) Histogram of degeneration of G856D-expressing thin and thick neurites at 30 days in culture. Note that degeneration occurs significantly more frequently in small-diameter (<3 μm) compared to large-diameter (>5 μm) neurites.
GFP: green fluorescent protein; DIV: days in vitro.

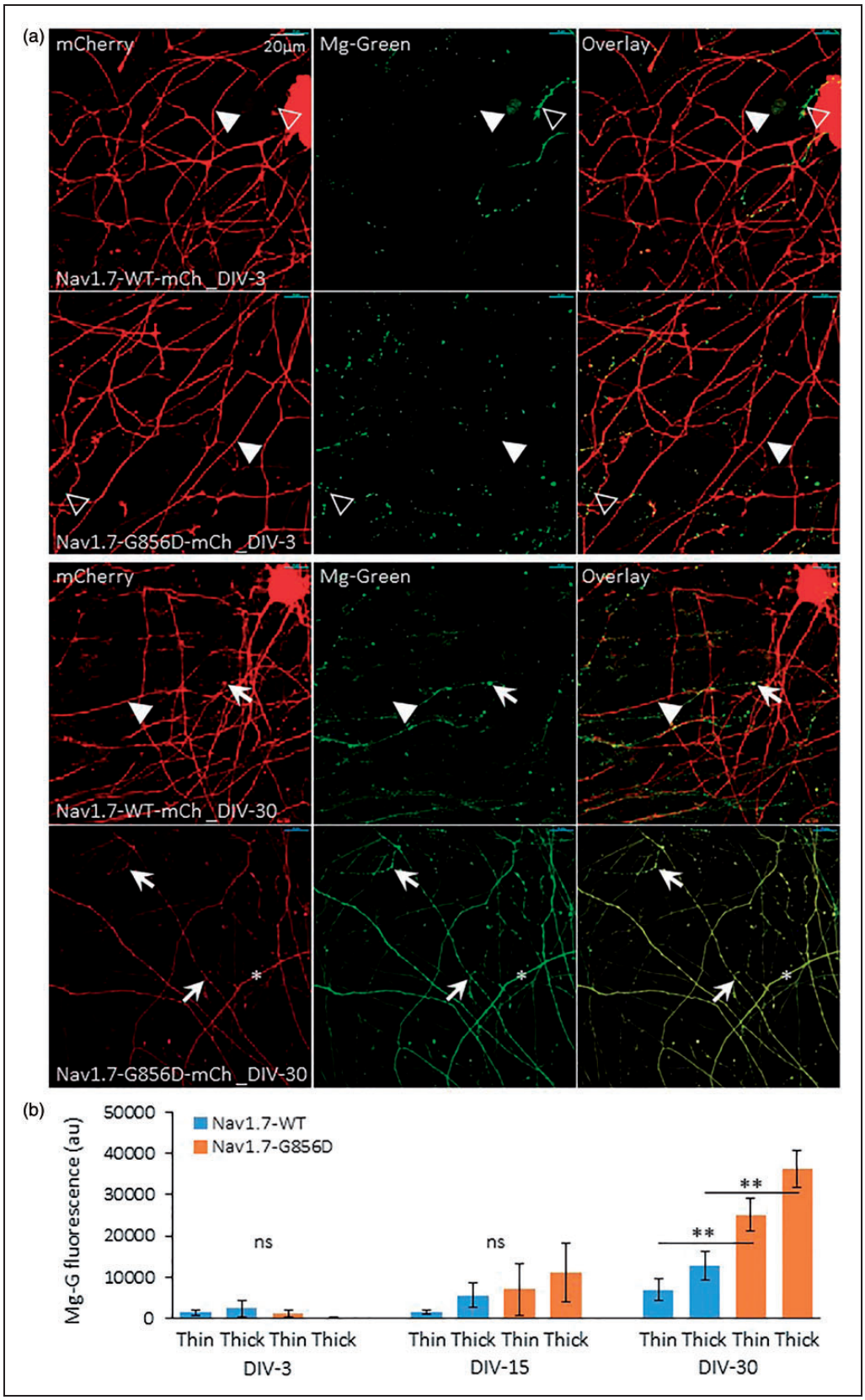

Figure 4. ATP levels in neurites expressing WT and G856D Nav1.7 channels. (a) Representative images showing the WT and G856D expressing neurites and co-transfected with mCherry reporter (red) and assayed with Magnesium Green, AM, fluorescence (green) of DRG neurons at three days (upper panels) and 30 days (lower panels) *in vitro*. MgGreen fluorescence inversely correlates with ATP levels.

neurites > 5.0 μm in diameter (thick), the average F_{340}/F_{380} value was 0.7922 ± 0.0319 for WT Nav1.7 and 0.7662 ± 0.0308 for G856D mutant Nav1.7 ($P = 0.5887$, Figure 3(b)). At 30 DIV, the average F_{340}/F_{380} value for thin neurites was 0.8257 ± 0.0263 for WT Nav1.7 and 0.9525 ± 0.0194 for G856D mutant Nav1.7 ($P = 0.0082$, Figure 3(c)), while for thick neurites, the average F_{340}/F_{380} value was 0.6598 ± 0.0443 for WT Nav1.7 and 0.6461 ± 0.0728)for G856D mutant Nav1.7 ($P = 0.8801$, Figure 3(c)). Differences in F_{340}/F_{380} values were not significant for neuronal cell bodies that were either transfected or nontransfected with WT or G856D constructs (Figure 3(c)).

Time-dependent decrease in ATP levels in neurites expressing G856D Nav1.7 mutant channels

Previous studies have linked neurite injury due to Na^+/K^+-ATPase run-down with sodium channel activity in an *in vitro* model of mitochondrial compromise in DRG neurons.[21] However, ATP levels have not been assessed in painful neuropathy due to Nav1.7 mutations. Utilizing MgGreen as an indicator, with fluorescence intensity that inversely correlates with ATP levels, we assayed ATP levels from healthy appearing neurites (with no signs of degeneration) from WT and G856D-expressing DRG neurons. At 3 and 15 DIV, the average values for MgGreen fluorescence were not significantly different between WT and G856D expressing neurites (3 days: WT thin $= 1484 \pm 652$, G856D thin $= 1160 \pm 767$; WT thick $= 2370 \pm 1888$, G856D thick $= 217 \pm 159$; 15 days: WT thin $= 1593 \pm 502$, G856D thin $= 6975 \pm 6249$; WT thick $= 5624 \pm 2927$, G856D thick $= 11057 \pm 7120$; $P =$ ns for both thin and thick neurites, Figure 4(a) and (b)). In contrast, at 30 DIV, the average value of MgGreen fluorescence was significantly greater in neurites (both thin and thick) expressing G856D mutant channels in comparison to neurites expressing WT channels (30 days: WT thin $= 6939 \pm 2648$, G856D thin 25100 ± 4068, WT thick $= 12756 \pm 3535$, G856D thick $= 36239 \pm 4369$; $P = 0.0096$ for thin and $P = 0.0058$ for thick neurites, Figure 4(a) and (b)), indicating lower levels of ATP in G856D expressing neurites as compared to WT expressing neurites.

Elevated ROS level in neurites expressing G856D Nav1.7 channels

We next measured ROS levels from healthy appearing neurites by utilizing a cell permeable variant of the general oxidative stress indicator CM-H2DCFDA, which after oxidation by ROS produces green fluorescence. In parallel to the results of ATP analysis, the CM-H2DCFDA fluorescence values between WT and G856D expressing neurites were not significantly different at 3 and 15 DIV (3 days: WT thin 2381 ± 2639, G856D thin $= 1452 \pm 989$; WT thick $= 1085 \pm 977$, G856D thick $= 1540 \pm 1319$; 15 days: WT thin 198 ± 233, G856D thin $= 335 \pm 484$; WT thick $= 9174 \pm 7720$, G856D thick $= 1012 \pm 1579$; $P =$ ns for both thin and thick neurites, Figure 5(a) and (b)). At 30 days in culture, the CM-H2DCFDA fluorescence was significantly greater in neurites (both thin and thick) expressing G856D mutant channels as compared to neurites expressing WT channels (30 days: WT thin $= 19014 \pm 4304$, G856D thin $= 72421 \pm 18000$; WT thick $= 18942 \pm 5160$, G856D thick $= 82828 \pm 21064$; Figure 5(a) and(b)).

Discussion

SFN is a disorder associated with injury to peripheral unmyelinated C-fibers and thinly myelinated Aδ-fibers and loss of IENF and is clinically characterized by burning pain and dysautonomia.[1,2,4,24,25] Although SFN often occurs in the context of underlying disorders that include diabetes mellitus, impaired glucose tolerance, HIV infection, cancer chemotherapy, and other systemic diseases, in a substantial percentage of patients SFN occurs in the absence of an identifiable non-genetic cause.[2,3,5,7] Faber et al.[7] recently reported gain-of-function mutations in SCN9A (the gene encoding sodium channel Nav1.7) in nearly 30% of patients meeting stringent criteria for idiopathic SFN. Subsequently, additional gain-of-function mutations in SCN9A have been identified in patients with idiopathic SFN.[8,26] Gain-of-function mutations have also been identified in SCN10A (the gene encoding Nav1.8)[10–12] and SCN11A (the gene encoding Nav1.9)[13,14] in patients with idiopathic SFN.

Figure 4. Continued

Small arrowheads indicate transfected neurites with low MgGreen fluorescence, large arrowheads point to untransfected neurites with high MgGreen fluorescence, and arrows point to degenerating transfected neurites with high MgGreen fluorescence. The asterisk marks a G856D expressing neurite that does not exhibit signs of degeneration. Note the increased frequency of neurites with a high MgGreen signal at 30 days in culture that express G856D compared to WT expressing neurites, or to WT and G856D expressing neurites at three days in culture. (b) Histogram showing the average values of MgGreen fluorescence at 3 days, 15 days, and 30 days in vitro of thin (<3.0 μm) and thick (>5.0 μm) neurites expressing WT and G856D channels. MgGreen flurorescence is low, and differences are not statistically significant between WT and G856D expressing neurites at 3 days and 15 days. In contrast, at 30 days in culture, both thin and thick neurites expressing G856D Nav1.7 exhibit significantly higher MgGreen fluorescence levels in comparison to neurites expressing WT Nav1.7 ($P = 0.0096$ for thin and $P = 0.0058$ for thick nerve fibers).

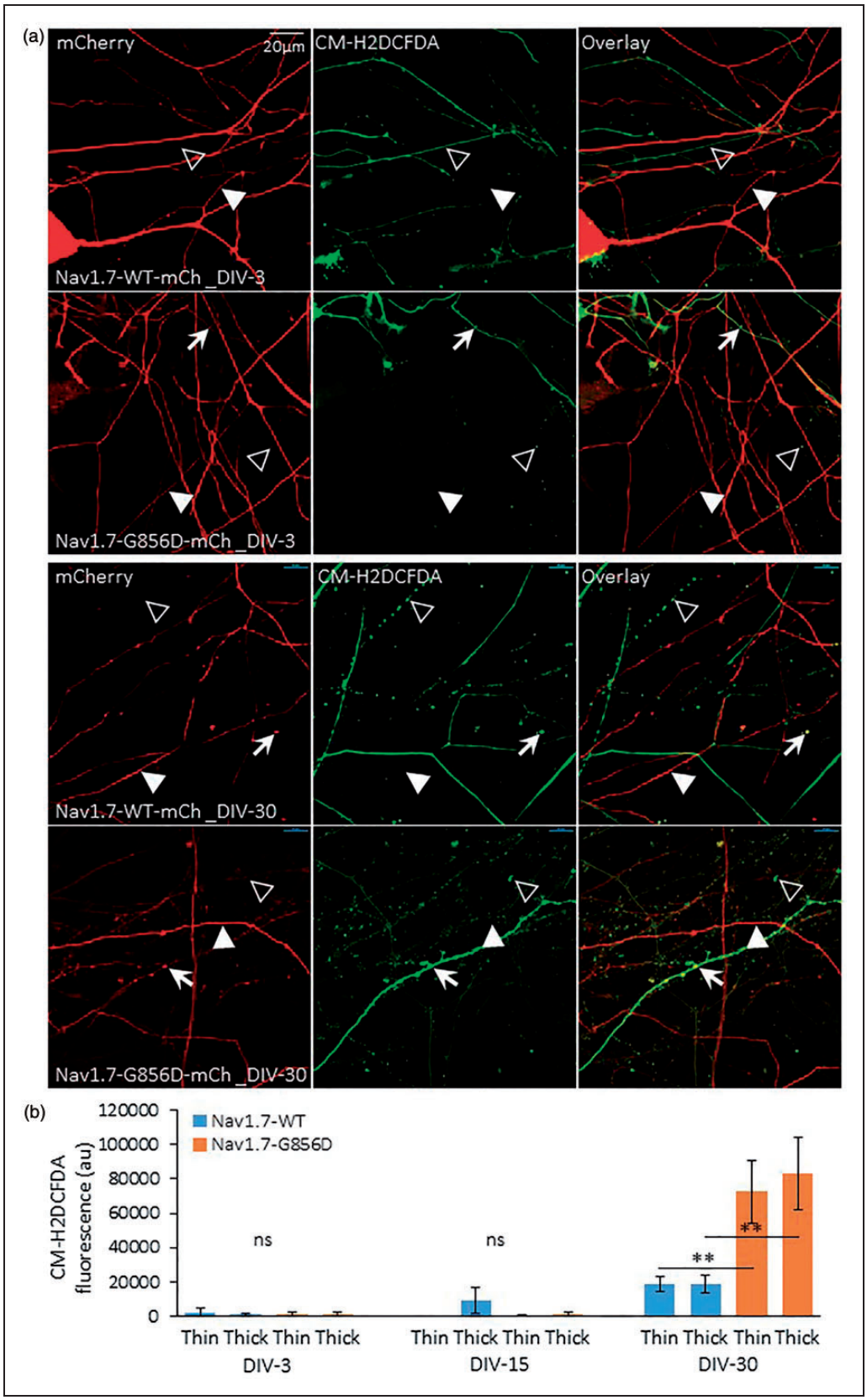

Figure 5. Oxidative stress in neurites expressing Nav1.7. (a) Representative images showing WT and G856D expressing neurites co-transfected with mCherry reporter (red) and labeled with CM-H2DCFDA (green) from DRG neurons at three days (upper panel) and 30 days (lower panel) *in vitro*. Small arrowheads point to transfected neurites with low fluorescence for CM-H2DCFDA, large arrowheads

However, molecular pathways that lead to degeneration in axons expressing gain-of-function mutations of sodium channels are incompletely understood, and the predilection for small-diameter axons has remained enigmatic.

Mutation G856D (c.2567G > A) in sodium channel Nav1.7, identified in SFN-affected individuals in a multi-generation family,[9] produces robust alterations of Nav1.7 channel biophysical properties when expressed in rat DRG neurons, hyperpolarizing channel activation by 10–15 mV, depolarizing voltage dependence of steady-state fast inactivation by 6.2 mV, slowing deactivation, and markedly enhancing ramp current and persistent current.[9] Current clamp analyses demonstrate a depolarized resting membrane potential and indicate that DRG neurons expressing G856D mutant channels are hyperexcitable, exhibiting decreased current threshold and increased spontaneous firing.[9]

To identify pathways that contribute to axonal dysfunction due to the G856D Nav1.7 mutation, we utilized an *in vitro* model system in which DRG neurons are transfected with WT or G856D Nav1.7 constructs. Using this *in vitro* model, we previously demonstrated that expression of another SFN-associated Nav1.7 mutant channel, I228M, significantly reduces mean neurite length at three days in culture.[27] In contrast, in the present study, mean neurite lengths of DRG neurons transfected with mutant G856D Nav1.7 constructs were not significantly different at three days in culture. However, there was a time-dependent reduction in the length of G856D-expressing neurites compared to WT neurites, with the mean neurite lengths of G856D-expressing neurons displaying a nearly 30% decrease compared to WT neurites at 30 days in culture. Paralleling the reduction in neurite lengths of G856D-expressing neurons, we observed a significantly increased percentage of neurites displaying signs of degeneration at 30 days. These observations in tissue culture suggest that the presence of mutant G856D Nav1.7 channels contributes in a time-dependent manner to dysfunction of neurite integrity. The time-dependent but relatively rapid time-course that we observed *in vitro* may have a clinical correlate. Although SFN typically begins to produce symptoms in adulthood, redness of the skin in the hands began at age 10, and distal limb pain began a few years later in the proband carrying the G856D mutation; on the basis of this history and the presence of acromesomelia (small distal limbs), Hoeijmakers et al.[9] suggested that dysfunction in peripheral axons expressing G856D mutant channels may have begun early in development. In this respect, the results in the present study mimic the relatively early onset and progression of SFN associated with the G856D mutation in humans and may provide an *in vitro* model of time-dependent axonal injury with a compressed time-course.

G856D mutant channels are notable in displaying a markedly enhanced persistent current,[9] which would be expected to result in a sustained Na^+ influx into the neurites. In early studies on rat optic nerve, Stys et al.[16] demonstrated that, under conditions of metabolic stress, persistent Na^+ influx through incompletely inactivating sodium channels can lead to reverse operation of the NCX, thereby importing damaging levels of Ca^{2+}. NCX and Nav1.7 channels have previously been shown to be expressed along the entire lengths of cultured DRG neuronal neuritis.[28] In our *in vitro* system, intracellular $[Ca^{2+}]_i$ levels at three days in culture were similar for WT and G856D-expressing neurites, both for smaller diameter (<3 μm) and larger diameter (>5 μm) neurites. At 30 days in culture, smaller diameter G856D-expressing neurites displayed significantly increased $[Ca^{2+}]_i$ compared to WT-expressing neurites, suggesting that increased Na^+ influx through G856D channels triggered reverse operation of NCX that resulted in increased $[Ca^{2+}]_i$. Consistent with this view, G856D-expressing neurites at 18 days in culture were shown to exhibit substantially greater basal levels of $[Ca^{2+}]_i$ than WT Nav1.7-expressing neurites, and inhibition of reverse mode NCX decreased basal intracellular $[Ca^{2+}]$ in G856D-expressing neuritis.[15] Larger diameter neurites did not exhibit the differential levels of $[Ca^{2+}]_i$ exhibited by small-diameter WT and G856D-expressing neurites, suggesting more robust $[Ca^{2+}]_i$ diffusion or homeostatic mechanisms in larger diameter neurites compared to smaller diameter neurites.

The increased levels of $[Ca^{2+}]_i$ in small-diameter neurites expressing G856D channels would be expected to have adverse consequences for neurite integrity. Increased intracellular levels of Ca^{2+} have been linked to the onset of degradative cascades leading to axonal

Figure 5. Continued

point to untransfected neurites with high CM-H2DCFDA fluorescence, and arrows point to degenerating transfected neurites with high CM-H2DCFDA fluorescence. Note the increased frequency of neurites with high fluorescence intensity for CM-H2DCFDA at 30 days in culture that express G856D Nav1.7 compared to neurites that express WT channels at 30 days, or to WT and G856D transfected neurites at three days in culture. (b) Histogram showing the average values for CM-H2DCFDA fluorescence at 3 days, 15 days, and 30 days in vitro of thin (<3.0 μm) and thick (>5.0 μm) neurites. Average values of CM-H2DCFDA are not significantly different between WT and G856D expressing neurites at 3 days and 15 days in vitro for either thin or thick neurites. In contrast, at 30 days in culture, average fluorescent levels for both thin and thick neurites expressing G856D are significantly higher than that for neurites expressing WT Nav1.7.

degeneration.[29,30] In addition to elevated levels of intracellular [Ca^{2+}] activating Ca^{2+}-sensitive calpains and phospholipases, Ca^{2+} levels play a key role in mitochondrial function, including mobility and production of ATP and ROS. Differential sensitivity of small-diameter axons to gain-of-function mutations of sodium channels is not entirely unexpected. Intracellular ionic concentrations within small-diameter unmyelinated axons would be anticipated to be particularly vulnerable to perturbations caused by ion channel activity, due to their high surface-to-volume ratios, high input impedance, and short diffusional and electrotonic length constant, and thus would be predicted to require substantial activity of the Na^+/K^+-ATPase to maintain ionic gradients.[19,20]

Our observations demonstrated reduced levels of ATP and increased levels of ROS in neurites expressing G856D channels. There was a time-dependent decrease in ATP (increased MgGreen fluorescence) and increase in ROS in G856D-expressing neurites compared to WT-expressing neurites. Interestingly, a syndrome of burning feet/burning hands has been described in human subjects with chronic mountain syndrome living at altitudes of >4000 m.[31] The magnitude of these symptoms, which are similar to those in SFN, was inversely correlated with levels of Na^+/K^+-ATPase measured in sural nerve biopsies.[32] Persson et al.[21] showed that sodium channel blockade attenuated the degeneration of neurites of DRG neurons induced with the ATPase inhibitor ouabain and demonstrated a similar protective effect with blockade of reverse sodium-calcium exchange, providing a mechanistic link between sodium channel activity, reverse sodium-calcium exchange, and axon injury due to run-down of ATPase.

Taken together, our observations support the notion that the presence of G856D Nav1.7 channels places an accumulating burden on DRG neurite integrity. Enhanced Na^+ influx through G856D channels is likely to exert two major effects: (1) an increased demand for Na^+/K^+-ATPase activity to maintain ionic gradients in neurites and (2) a reversal of NCX with import of Ca^{2+} leading to sustained elevated levels of $[Ca^{2+}]_i$. In both cases, demand for energy supplies would be anticipated to increase. Particularly in smaller diameter neurites, with increasing time, rising $[Ca^{2+}]_i$ levels might trigger mitochondrial dysfunction, further compounding a time-dependent increase in intracellular calcium levels that could enhance activity in degradative pathways and culminate in neurite degeneration with a predilection for small-diameter nerve fibers.

Acknowledgment

The Center for Neuroscience and Regeneration Research is a collaboration of the Paralyzed Veterans of America with Yale University.

Author contributions

HR, SL, and JAB performed experiments; HR, JAB, and SGW analyzed data; HR, JGJH, CGF, ISJM, GL, JAB, and SGW interpreted results of experiments; HR prepared figures; HR, SL, JGJH, CGF, ISJM, GL, JAB, and SGW approved final version of manuscript; HR, CGF, ISJM, JAB, and SGW edited and revised manuscript; and HR, JAB, and SGW contributed to the conception and design of research.

Declaration of Conflicting Interests

The author(s) declared no potential conflicts of interest with respect to the research, authorship, and/or publication of this article.

Funding

The author(s) disclosed receipt of the following financial support for the research, authorship, and/or publication of this article: This work was supported in part by the Rehabilitation Research Service (SGW) and Medical Research Serve (SGW) from the Department of Veterans Affairs and by the European Union 7th Framework Program FP7/2007–2013 (Grant 602273).

References

1. Lacomis D. Small-fiber neuropathy. *Muscle Nerve* 2002; 26: 173–188.
2. Devigili G, Tugnoli V, Penza P, et al. The diagnostic criteria for small fibre neuropathy: from symptoms to neuropathology. *Brain* 2008; 131: 1912–1925.
3. Bednarik J, Vlckova-Moravcova E, Bursova S, et al. Etiology of small-fiber neuropathy. *J Peripher Nerv Syst* 2009; 14: 177–183.
4. Hoeijmakers JG, Faber CG, Lauria G, et al. Small-fibre neuropathies–advances in diagnosis, pathophysiology and management. *Nat Rev Neurol* 2012; 8: 369–379.
5. Lauria G, Merkies IS and Faber CG. Small fibre neuropathy. *Curr Opin Neurol* 2012; 25: 542–549.
6. McArthur JC. Painful small fiber neuropathies. *Continuum (Minneap Minn)* 2012; 18: 106–125.
7. Faber CG, Hoeijmakers JG, Ahn HS, et al. Gain of function Nav1.7 mutations in idiopathic small fiber neuropathy. *Ann Neurol* 2012; 71: 26–39.
8. Han C, Hoeijmakers JG, Ahn HS, et al. Nav1.7-related small fiber neuropathy: impaired slow-inactivation and DRG neuron hyperexcitability. *Neurology* 2012; 78: 1635–1643.
9. Hoeijmakers JG, Han C, Merkies IS, et al. Small nerve fibres, small hands and small feet: a new syndrome of pain, dysautonomia and acromesomelia in a kindred with a novel NaV1.7 mutation. *Brain* 2012; 135: 345–358.
10. Faber CG, Lauria G, Merkies IS, et al. Gain-of-function Nav1.8 mutations in painful neuropathy. *Proc Natl Acad Sci U S A* 2012; 109: 19444–19449.
11. Huang J, Yang Y, Zhao P, et al. Small-fiber neuropathy Nav1.8 mutation shifts activation to hyperpolarized potentials and increases excitability of dorsal root ganglion neurons. *J Neurosci* 2013; 33: 14087–14097.

12. Han C, Vasylyev D, Macala LJ, et al. The G1662S NaV1.8 mutation in small fibre neuropathy: impaired inactivation underlying DRG neuron hyperexcitability. *J Neurol Neurosurg Psychiatry* 2014; 85: 499–505.
13. Huang J, Han C, Estacion M, et al. Gain-of-function mutations in sodium channel Na(v)1.9 in painful neuropathy. *Brain* 2014; 137: 1627–1642.
14. Han C, Yang Y, de Greef BT, et al. The Domain II S4-S5 Linker in Nav1.9: a missense mutation enhances activation, impairs fast inactivation, and produces human painful neuropathy. *Neuromolecular Med* 2015; 17: 158–169.
15. Estacion M, Vohra BP, Liu S, et al. Ca^{2+} toxicity due to reverse Na^{+}/Ca^{2+} exchange contributes to degeneration of neurites of DRG neurons induced by a neuropathy-associated Nav1.7 mutation. *J Neurophysiol* 2015; 114: 1554–1564.
16. Stys PK, Waxman SG and Ransom BR. Ionic mechanisms of anoxic injury in mammalian CNS white matter: role of Na^{+} channels and Na^{+}-Ca^{2+} exchanger. *J Neurosci* 1992; 12: 430–439.
17. Stys PK. General mechanisms of axonal damage and its prevention. *J Neurol Sci* 2005; 233: 3–13.
18. Gøransson LG, Mellgren SI, Lindal S, et al. 2004) The effect of age and gender on epidermal nerve fiber density. *Neurology* 2004; 62: 774–777.
19. Waxman SG, Black JA, Kocsis JD, et al. Low density of sodium channels supports action potential conduction in axons of neonatal rat optic nerve. *Proc Natl Acad Sci USA* 1989; 86: 1406–1410.
20. Donnelly DF. Spontaneous action potential generation due to persistent sodium channel currents in simulated carotid body afferent fibers. *J Appl Physiol* 2008; 104: 1394–1401.
21. Persson AK, Kim I, Zhao P, et al. Sodium channels contribute to degeneration of dorsal root ganglion neurites induced by mitochondrial dysfunction in an in vitro model of axonal injury. *J Neurosci* 2013a; 33: 19250–19261.
22. Pool M, Thiemann J, Bar-Or A, et al. NeuriteTracer: a novel ImageJ plugin for automated quantification of neurite outgrowth. *J Neurosci Methods* 2008; 168: 134–139.
23. Leyssens A, Nowicky AV, Patterson L, et al. The relationship between mitochondrial state, ATP hydrolysis, [Mg2+]i and [Ca2+]i studied in isolated rat cardiomyocytes. *J Physiol* 1996; 496(Pt 1): 111–128.
24. Gorson KC and Ropper AH. Idiopathic distal small fiber neuropathy. *Acta Neurol Scand* 1995; 92: 376–382.
25. Holland NR, Crawford TO, Hauer P, et al. Small-fiber sensory neuropathies: clinical course and neuropathology of idiopathic cases. *Ann Neurol* 1998; 44: 47–59.
26. Hoeijmakers JG, Merkies IS, Gerrits MM, et al. Genetic aspects of sodium channelopathy in small fiber neuropathy. *Clin Genet* 2012; 82: 351–358.
27. Persson AK, Liu S, Faber CG, et al. Neuropathy-associated Nav1.7 variant I228M impairs integrity of dorsal root ganglion neuron axons. *Ann Neurol* 2013b; 73: 140–145.
28. Persson AK, Black JA, Gasser A, et al. Sodium-calcium exchanger and multiple sodium channel isoforms in intraepidermal nerve terminals. *Mol Pain* 2010; 6: 84.
29. Stirling DP and Stys PK. Mechanisms of axonal injury: internodal nanocomplexes and calcium deregulation. *Trends Mol Med* 2010; 16: 160–170.
30. Wang JT, Medress ZA and Barres BA. Axon degeneration: molecular mechanisms of a self-destruction pathway. *J Cell Biol* 2012; 196: 7–18.
31. Thomas PK, King RH, Feng SF, et al. Neurological manifestations in chronic mountain sickness: the burning feet-burning hands syndrome. *J Neurol Neurosurg Psychiatry* 2000; 69: 447–452.
32. Appenzeller O, Thomas PK, Ponsford S, et al. Acral paresthesias in the Andes and neurology at sea level. *Neurology* 2002; 59: 1532–1535.